IEEE Access
Multidisciplinary ⋮ Rapid Review ⋮ Open Access Journal

Received 6 December 2022, accepted 3 January 2023, date of publication 9 January 2023, date of current version 19 January 2023.

Digital Object Identifier 10.1109/ACCESS.2023.3234996

RESEARCH ARTICLE

Robust Speed Controller for PMSG Wind System Based on Harris Hawks Optimization via Wind Speed Estimation: A Real Case Study

NOURA A. NOUR ALDIN[1], WALID S. E. ABDELLATIF[1], Z. M. SALEM ELBARBARY[2,3], AHMED I. OMAR[4], AND MOHAMED METWALLY MAHMOUD[5]

[1]Electrical Department, Faculty of Technology and Education, Suez University, Suez 8151650, Egypt
[2]Electrical Engineering Department, College of Engineering, King Khalid University, Abha 61421, Saudi Arabia
[3]Electrical Engineering Department, Faculty of Engineering, Kafr El-Sheikh University, Kafr El-Sheikh 33516, Egypt
[4]Electrical Power and Machines Engineering Department, The Higher Institute of Engineering at El-Shorouk City, El-Shorouk Academy, Cairo 11837, Egypt
[5]Electrical Engineering Department, Faculty of Energy Engineering, Aswan University, Aswan 81528, Egypt

Corresponding authors: Ahmed I. Omar (a.omar@sha.edu.eg) and Mohamed Metwally Mahmoud (metwally_m@aswu.edu.eg)

This work was supported by the Deanship of Scientific Research, King Khalid University, under Grant RGP.1/223/43.

ABSTRACT Modern wind power systems have recently tended to focus on achieving fast-tracking wind speeds (WSs), high maximum power point tracking (MPPT) efficacy without mechanical sensors, and high performance under uncertain WS together with an effective control system. Therefore, a sensorless MPPT method is introduced, which calculates the actual WS to save system installation costs and boost performance levels. The implemented MPPT method is based on the approximating of the 3-order polynomial to the aerodynamics torque power coefficient. In this study, three-speed control strategies (SCSs) for a grid-connected permanent magnet synchronous wind generator (PMSWG) are examined and assessed. Harris Hawks' algorithm (HHA)-based PI controller (HHA-PIC) is used in place of (the conventional proportional-integral controller (CPIC), and adaptive fuzzy logic controller (AFLC)) as a speed controller to overcome their drawbacks. To track the generator speed to the desired speed, the HHA-PIC is used. All the CPIC, AFLC, and HHA-PIC have been carefully thought out and constructed to satisfy the speed control loop's responsive performance. Additionally, a comparison of SCSs amongst the categories under investigation is done. The effect of HHA on the functionality of SCS is verified using MATLAB/SIMULINK. To ensure the efficacy and supremacy of the HHA-PIC over the CPIC and AFLC, a wide variety of WSs (step change, ramp, and real fluctuations) are applied. The HHA-PIC boosts system efficiency over AFLC and CPIC by 0.81% and 8.48%, respectively. Finally, it can be said that HHA is a crucial remedy for the problems with CPIC and is superior to AFLC.

INDEX TERMS Adaptive FLC, efficiency, Harris Hawks' algorithm (HHA), MPPT, PMSG, real wind variations, wind speed estimation.

I. INTRODUCTION

In the domains of international politics, economics, science, and technology, there is now widespread agreement that greenhouse gas (GG) emissions must be controlled and the effects of global warming must be mitigated. The overuse and use of fossil fuels (FFs) by humans is the primary cause of the buildup of GGs, particularly CO_2, in the atmosphere. The overall global use of FFs and CO_2 emissions in 2019 were 583.9 exajoules and 34169.0 million tonnes, respectively, per the BP Statistical Review of World's energy 2020 [1], [2]. Roughly 5.0% of the world's energy is produced by renewable generators, hydroelectricity and nuclear power being the exceptions. Approximately 1% each year, or 340 million tonnes per year, more CO_2 is still being released into the atmosphere [3], [4]. Energy from renewable sources

The associate editor coordinating the review of this manuscript and approving it for publication was Ton Duc Do.

(EFRSs), particularly wind energy (WE), have been used to address these issues as environmental dangers were more widely known and there was a goal to limit the use of fossil fuels [5], [6], [7]. It is constantly expanding to meet the rising demand for power in the world due to its clean and environmental dangers [8]. As a result, it is anticipated to supply 20% of the world's energy demand by 2030 [9], [10].

Fixed speed (FS) and variable speed (VS) are the two basic principles used in worldwide WE marketing. The FS generators are straightforward and cost-effective, but they require a gearbox and have a limited speed range. Globally expanded VS eliminates the need for a gearbox and enables maximum power harvest regardless of wind speed (WS) [11], [12]. The VS uses a variety of machine types, including permanent magnet synchronous wind generators (PMSWGs), doubly fed induction wind generators, and squirrel cage induction wind generators [13], [14]. The PMSWG has numerous advantages compared to the other sorts described, including excellent performance and power density as well as great reliability and efficiency. Additionally, removing the gearboxes and DC excitation increases the WE unit efficiency by 10% [11], [13]. Lately, 3-phase PMSWGs have been used in a variety of industries to improve fault tolerance while reducing phase current and torque pulsation ratio [15]. The main shortcomings of these technologies continue to be their expensive power converters and intricate control mechanisms [16].

To assure utilizing all accessible energy at fluctuating WSs, maximum power point tracking (MPPT) methods were researched [17], [18], [19]. Precise WS measurement is necessary in an MPPT setup in order to properly control the mechanical speed and achieve the desired value. A variety of anemometers having precision and quality of (5–10) % are placed at various locations near the turbine region in order to measure the WS. A perfect measurement of the effective WS is necessary for the turbine to be controlled effectively; however, the anemometer is unable to provide this information. Additionally, the anemometer has a high upfront and ongoing cost, which lowers total system durability [20], [21], [22]. WS estimation (WSE) methods are being used instead of sensors because they reduce system complexity, increase efficiency, and deliver precise WS measurements. In [17] and [23], various WSE approaches were discussed. The polynomial-based estimating (PBE) technique is one of them and is straightforward and precise [17], [24]. Thus, it is taken into account here just to calculate the WS.

Due to the necessity of energy these days, a lot of time and effort has been put into the MPPT research area for WE systems. The majority of these studies used traditional algorithms like P&O and modified P&O, while other studies used metaheuristic optimization techniques to optimize either the PIC or the artificial neural network-based controller. A study that compared two methods (P&O and HCS), for a hybrid PV/WE technology was presented in [25]. To power, the WE-producing system, a brushless power split system was introduced, and a comparison with a single MPPT was made [26]. The use of a new MPPT technique based on adaptive active fault tolerant control solved some issues that came with the operation of WE generation [27]. A fractional control mechanism for adjusting the WE system's pitch angle to maximize the power it produces was presented in [28] and compared with the traditional PI sort. Installing fuzzy logic control (FLC) for MPPT increased the system harvest power and system efficiency [29]. As an approach to maximize the power produced by the WE system, a neural network (NN) with a radial basis function was presented [30]. Additionally, a modified particle swarm optimizer (PSO) was employed to implement the learning process while the gradient descent technique was used to train the NN.

An MPPT technique with changeable step sizes by perturbing the ω_r of the WE system was established in [31]. A self-adaptive P&O strategy for MPPT integrated with the WE system was described in [32], to increase its output power (P). A contrast with FLC, variable P&O, and fixed step P&O was made in this study to increase the P, adaptive P&O, and hybrid P&O control approaches for MPPT fitted with WE systems were given in [33]. Control of the MPPT fitted with the WE system by choosing a slide mode extremum was done in [34]. The settings of the built-in controller were optimized using an upgraded invasive weed method. In [35], two MPPT techniques: λ and optimum torque control (OTC) were installed in WE arrangement and assessed. For the purpose of replicating MPPT for WE systems, [36] demonstrated a hybrid technique integrating HCS and power signal feedback control, and the PIC was optimized using PSO. Reference [37] used NN with reinforcement learning to act out MPPT for the WE system. For the MPPT-WE system, a dsPIC30F4011 was established in [38]. In order to simulate MPPT implemented in the WE system in Saudi Arabia, [39] proposed a method built on a grasshopper optimizer (GOA). In comparison to other optimizers, the GOA managed the boost converter duty cycle to increase P.

Various controllers can be divided into several sorts, like linear, nonlinear, or predictive. It is possible for controllers to adjust the required regulated variables and enhance the whole dynamic system. Though economical and easy to build, linear controllers have several drawbacks, including poor dynamic response, poor efficacy, and high sensitivity to outside disruptions [40], [41]. The continuous model predictive controller (MPC) and the finite control set MPC are two forms of MPCs that are effective at predicting and enhancing system behavior, however, MPC is quite complex and requires a lot of computations [42], [43]. To create the converter switching signals in continuous mode, a modulator is required, however in the alternate mode, this is not necessary [44]. To obtain the MP of the WE system, MPC-based MPPT was proposed in [45]. An MPPT for a WE system utilizing a PIC that had its tracking speed increased employing an ant colony optimizer was built in [46]. The use of metaheuristic algorithms is still limited and requires more attention, despite the large number of applied methods used to simulate MPPT with WE systems.

Additionally, hill-climbing search algorithms may not be successful in extracting the MPP and have some restrictions on tracking speed and efficiency. The most modern optimization techniques, including, swarming methods, and the Elliptic Curve, have been successfully used to regulate various controlled variables including torque and current in a variety of engineering challenges. In both the machine and grid side, pitch control loops, optimized controllers were employed instead of the conventional proportional-integral controller (CPIC) [47], [48].

An effective metaheuristic strategy harris hawk's algorithm (HHA) is employed to close the gap left by the usage of the earlier techniques. In this work, the optimal power output of a PMSWG is investigated for a variety of WS profiles (step change, ramp changes, and real fluctuations). Without employing any sensors, the effective WS is estimated via the WSE technique. Additionally, it lowers the cost of system installation, gets rid of WE system complexity, raises reliability, and boosts efficiency. Numerous disadvantages of employing a CPIC as a speed controller directly impact the WE system's dynamic response. The CPIC of the speed control loop (SCL) is fine-tuned using the HHA to reduce these limitations. The adaptive fuzzy logic controller (AFLC) is designed and implemented as a speed controller to highlight the merits of the proposed system. To monitor the machine speed to the reference amplitude, the HHA-PIC is used. The CPIC, AFLC, and the HHA-PIC are all well thought out and developed to guarantee the SCL's obedient behavior. The transfer function (TF) notion is used in the formulation of the PIC gains. Additionally, an illustration scheme is used to demonstrate the HHA design. Additionally, a comparison of SCLs amongst the categories under research is conducted.

The following is how this paper is formed: The WE system mathematical model and control are presented in Section II. Section III provides a description of the WSE algorithm. Section IV provides clarification on the SCLs and HHA. Simulation results are presented in Section V. In the final section (VI), the work's result is reported.

II. STUDIED SYSTEM MODEL AND CONTROL

Fig. 1 shows the researched system and its control system. An exterior SCL and two inner current control loops make up the wind-side converter (WSC). SCL is in charge to control the generator\mechanical\rotor speed (ω_r), and the current control loops are applied for maximizing the generated power. The back-to-back power electronic converter connects the PMSWG to the electric grid (EG), and the grid-side converter injects output power (P) into the EG.

A. WIND TURBINE (WT) MODEL

The produced mechanical power (P_m), tip speed ratio (λ), power coefficient (C_p), and mechanical torque (T_m) for the turbine model can be formulated as follows [49], [50], [51]:

$$P_m = C_p\left(\lambda.\beta\right)\frac{A\rho v_w^3}{2} \tag{1}$$

$$C_p(\lambda,\beta) = 0.5176\left(\frac{116}{\lambda_i} - 0.4\beta - 5\right)e^{\frac{-21}{\lambda_i}} + 0.0068\lambda \tag{2}$$

$$\lambda = \frac{\omega_r R}{v_w} \tag{3}$$

$$\frac{1}{\lambda_i} = \frac{1}{\lambda + 0.08\beta} - \frac{0.035}{1+\beta^3} \tag{4}$$

$$T_m = \frac{P_m}{\omega_r} \tag{5}$$

where ρ, β, A, and v_w are the air density, pitch angle, blades area, and WS, respectively.

Fig. 2 depicts the four operational zones of the WE system broken down into these regions. The turbine is restricted from operating in areas 0 and 3 to protect it from any mechanical dangers. The MPPT runs in region 1 just under-rated WS to maximize the power generated at various WSs. In all other cases, the pitch control is used to ensure that the turbine is operated safely over the allowed WS until the cutout amplitude. As shown in Fig. 3, the ω_r is adjusted to track the MPP at any WS to function with the ideal values of, λ, C_p, and β.

B. PMSWG MODEL

The PMSWG's model is fully defined in [50], [52], and [53] and its stator voltages (V_{ds} and V_{qs}) are presented via Park's transformation:

$$\begin{bmatrix} V_{ds} \\ V_{qs} \end{bmatrix} = [R_s]\begin{bmatrix} I_{ds} \\ I_{qs} \end{bmatrix} + \begin{bmatrix} \lambda_d' - \omega_e\psi_q \\ \lambda_q' - \omega_e\psi_d \end{bmatrix} \tag{6}$$

where $\dot{\lambda_d} = L_{ds}\frac{dI_d}{dt}$, $\dot{\lambda_q} = L_{qs}\frac{dI_q}{dt}$, and the subscript "s" denotes stator.

The symbols R_s, (I_{ds}, I_{qs}), ω_e, *and* (L_{ds}, L_{qs}) are the resistance, currents, electrical angular speed, and inductances, respectively.

The flux components are written as:

$$\psi_{ds} = L_{ds}I_{ds} + \psi_{pm} \tag{7}$$

$$\psi_{qs} = L_{qs}I_{qs} \tag{8}$$

where ψ_{pm} is the permanent magnet (PM) flux linkage fundamental value.

The electromagnetic torque (T_e) can really be defined in the following way:

$$\begin{aligned} T_e &= \frac{3}{2}n_p\left(\psi_{ds}I_{ds} - \psi_{qs}I_{qs}\right) \\ &= \frac{3}{2}n_p\left(\psi_{pm}I_{qs} + I_{ds}I_{qs}\left(L_{ds} - L_{qs}\right)\right) \end{aligned} \tag{9}$$

For the surface-mounted PMs sort, (L_{ds}-L_{qs}). I_{ds} is set\forced to zero to remove losses. So, T_e will be written as:

$$T_e = \frac{3}{2}n_p\left(\psi_{pm}I_{qs}\right) \tag{10}$$

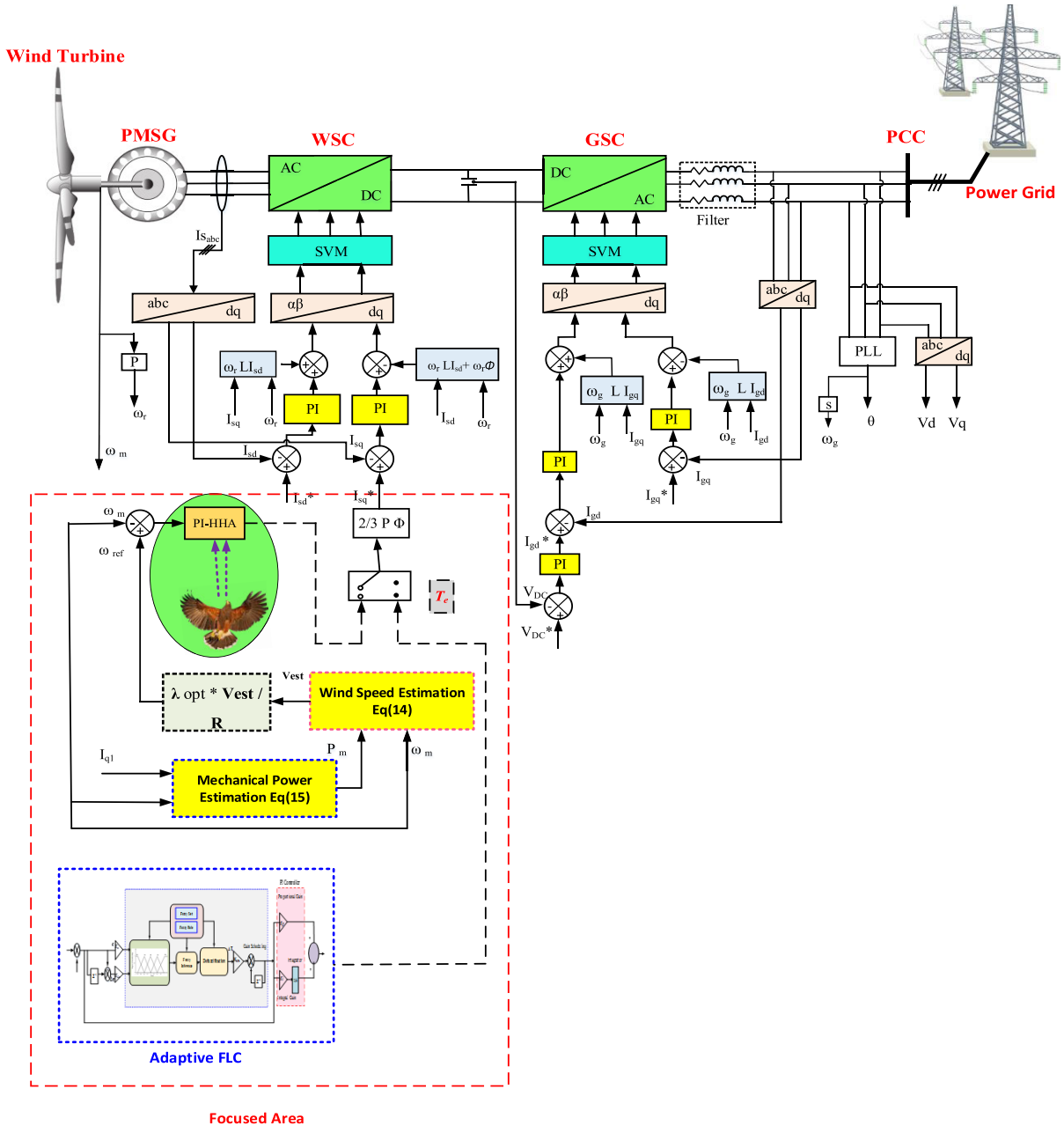

FIGURE 1. Addressed system.

The system's mechanical Eq. is written as in (11):

$$T_m = J\frac{d\omega_r}{dt} + f\omega_r + T_e \tag{11}$$

where f and J are the friction coefficient, and moment of inertia, respectively.

C. CONTROL OF WSC

Since SPL is a component of the WSC system, its control function is covered in this article. As seen in Fig. 1, the WSC's job is to maximize the power that the WS captures. To achieve optimum operation during the WS fluctuation, the MPPT is used. As seen in Figs. 2 and 3, its function is to achieve Cp = 0.48 and $\lambda = 8.1$ in zone 1 with $\beta = 0$. The WSC also uses two control loops to implement field-oriented control. The MPPT method is used to adjust ω_r at its desired value before applying the SPL. To reduce ω_r error, a variety of controller sorts, including traditional or improved PI controllers, are used as speed controllers. The inner one is in charge of producing the switching pulses and controlling the machine currently. The space vector modulation controls the machine current with its reference to enhance the produced T_e, which is linked to I_{qs} and forces I_{ds} to 0. Fig. 4 depicts the SCL concept in detail [12], [54], [55].

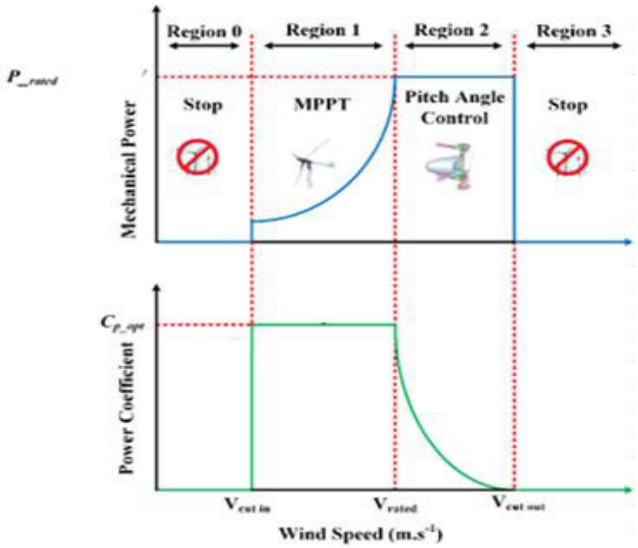

FIGURE 2. Operating regions of the wind system.

TABLE 1. Turbine constants.

Constants	Values
a_o	0.007 158 14
a_1	−0.044 540 63
a_2	0.028 992 77
a_3	−0.002 025 19

III. WSE ALGORITHM

With no anemometer, v_W is calculated from nonlinear 3-order polynomial C_p in (12) [56], [57].

$$C_p = a_0 + a_1\lambda + a_2\lambda^2 + a_3\lambda^3 \tag{12}$$

By substituting (1) and (3) into (12), the P_m is written as in (13).

$$P_m = \frac{\rho A v_w^3}{2}\left(a_o + a_1\frac{\omega_r R}{v_W} + a_2\left(\frac{\omega_r R}{v_W}\right)^2 + a_3\left(\frac{\omega_r R}{v_W}\right)^3\right) \tag{13}$$

v_W is calculated as a function of (P_m, ω_r) via the next 3-order polynomial Eq. (14), implementing a numerical analysis solution, and a single root is feasible from the three roots. The wind system constants are presented in Table 1 [56].

$$v_w^3 + \frac{a_1}{a_0}R\omega_r v_w^2 + \frac{a_2}{a_0}(R\omega_r)^2 v_w + \frac{a_3}{a_0}(\omega_r R)^3 - \frac{2P_m}{\rho A} = 0 \tag{14}$$

For calculating P_m as a function of (ω_r, I_{qs}), Eq. (15) is expressed as follows:

$$P_m = \omega_r\left(J\frac{d\omega_r}{dt} + f\omega_r + 1.5n_p\psi_{pm}I_{qs}\right) \tag{15}$$

IV. INVESTIGATED CONTROLLERS FOR SPEED LOOP

A. PI CONTROLLER

The SCL controls the ω_r at its ideal value, which is created by the WSE method, to harvest the greatest power for all WS changes. Therefore, a precise CPIC design by a thorough TF of the entire system is crucial. Using a 2-mass model, the TF has been calculated from the drive train's (DT) dynamics as a function of (ω_r, T_e). Through a spring and damper, the high-speed mass of the PMSWG is connected to the low-speed mass of the turbine. The linearization model is used to describe the 2-mass DT (16-19) [47], [56], [57],.

$$\frac{d\Delta\omega_r}{dt} = \frac{\Delta T_e + \Delta T_{sh}}{2H_g} \tag{16}$$

$$\frac{d\Delta\theta_r}{dt} = \omega_c\left(\Delta\omega_t - \Delta\omega_r\right) \tag{17}$$

$$\frac{d\Delta\omega_t}{dt} = \frac{\Delta T_m - \Delta T_{sh}}{2H_t} \tag{18}$$

$$\Delta T_{sh} = K_s\Delta\theta_r + f\left(\Delta\omega_t - \Delta\omega_r\right) \tag{19}$$

where the symbols (H_g, H_t), T_{sh}, ω_t, θ_r, (K_s,f) are the inertia constant of (generator and turbine), shaft torsional torque, turbine speed, shaft twist angle, shaft stiffness, and damping coefficients, respectively.

Both of P_m and wind-power (P_{wind}) can be written as:

$$P_m = P_{wind}C_p\left(\lambda, \beta\right) \tag{20}$$

$$P_{wind} = 0.5\rho\pi R^2 v_w^3 \tag{21}$$

Implementation of linearization concept around ω_r and from Eq. (5) ΔT_m is expressed as:

$$\Delta T_m \approx -\frac{P_{mo}}{\omega_{to}^2}\Delta\omega_t + \frac{P_{windo}}{\omega_{to}}\frac{C_p\left(\lambda, \beta\right)}{\lambda}\frac{d\lambda}{d\omega_t}\Delta\omega_t \tag{22}$$

The SCL schematic block diagram is presented in Fig. 5. $\frac{\alpha_\omega}{S+\alpha_\omega}$ is the inner current CL, α_ω is the converter's CL bandwidth. The controller gains ($K_{p(\omega)}$, $K_{i(\omega)}$) are designed as $\frac{K_{p(\omega)}}{2(H_t+H_g)} \ll \alpha_\omega$ and $\frac{K_{i(\omega)}}{K_{p(\omega)}} \ll \alpha_\omega$. The dynamics of the converter's CL are ignored when ($\omega \ll \alpha_\omega$). Therefore, the speed CL-TF is written as in (23).

$$\frac{\omega_r}{\omega_{ref}} = \frac{2s\omega_n\xi + \omega_n^2}{s^2 + 2s\omega_n\xi + \omega_n^2} \tag{23}$$

where ω_n, and ζ are the CL bandwidth, and the damming ratio of the PIC, respectively. Also, $\omega_n^2 = K\frac{K_{i(\omega)}}{2H_g}$, $2\omega_n\zeta = K\frac{K_{p(\omega)}}{2H_g}$, and $K = 1.5\mathrm{n_p}\psi_{\mathrm{pm}}\mathrm{T_{base}}$. The attained controller gains for precise operation based on this analysis are ($K_p = 5$, and $K_i = 100$).

B. ADAPTIVE FLC MPPT CONTROL

Due to its simplicity, ability to tackle system nonlinearity, and lack of information regarding mathematical modeling, FLC approaches are now more frequently used in a variety of applications [58]. Weird tracking behavior is caused by the nonlinearity of WE systems and climatic conditions. As a result, adaptive FLC-based MPPT techniques can be used to track the MPP in the PMSG WE system with less

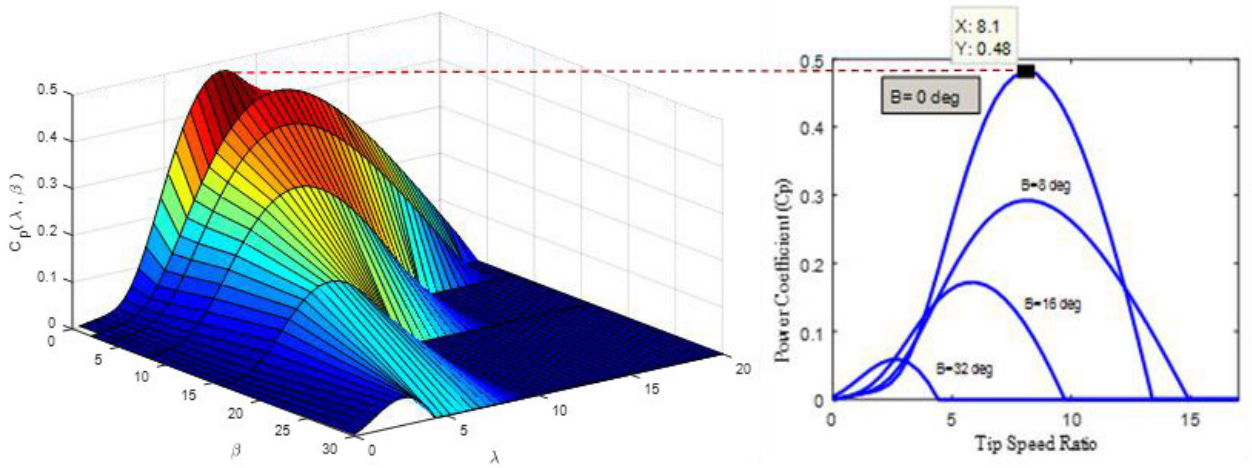

FIGURE 3. λ, *Cp* and β.

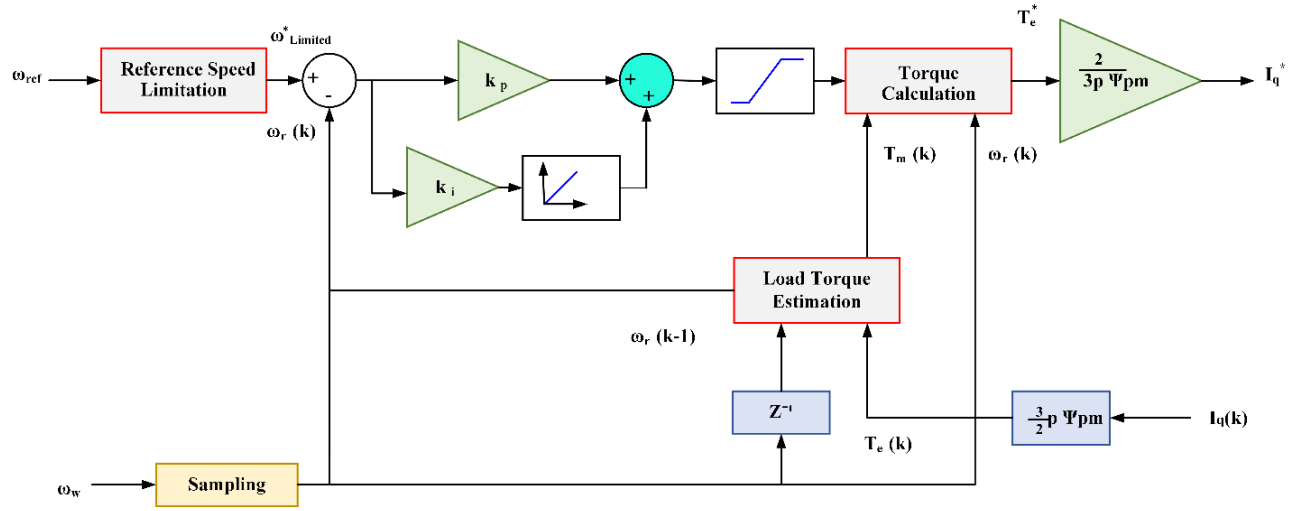

FIGURE 4. Speed control concept.

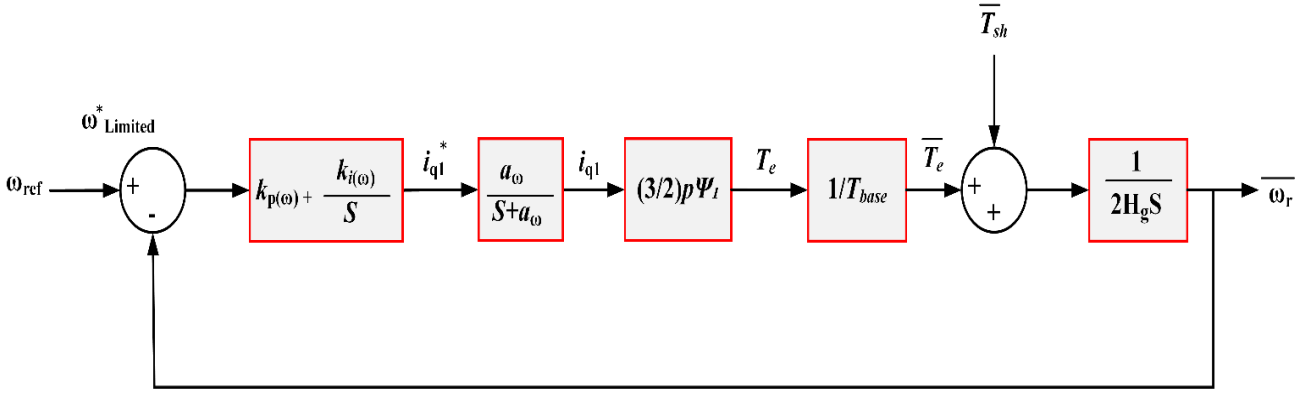

FIGURE 5. PI speed controller block diagram.

data needed and simpler implementation. For obtaining the MPPT in WE systems, numerous FLC methods have been proposed in the literature. There are three primary stages that the FLC's functioning and construction may be broken

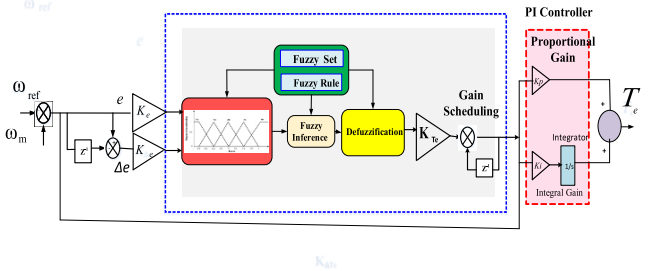

FIGURE 6. Adaptive FLC structure.

down into. These stages contain steps for fuzzing, evaluating rules, and defuzzification. Fig. 6 illustrates the reaction of the adaptive FLC adjustable parameters to system modifications, including output scaling factor, fuzzy rule, and membership function [29], [59]. Application of adaptive FLC can enable the PMSG to run at MPP as well as high dynamic performance under high variable wind speed. As a result, when providing a new control scheme superior to this recent scheme, is considered a robust, efficient, and effective approach.

C. HHA-PIC MPPT CONTROL

The HHA is a metaheuristic approach that mimics the HH's successful chase technique's cooperative behavior. Like other techniques, it contains the phases of exploration and exploitation. The HHA is broken down into two exploration phases and four exploitation steps in the formulas below. The following processes are employed by HHs to kill their rabbits and are mimicked and modeled by the HHA model. It was chosen for this research due when put to the test on 6 constrained design engineering tasks and 29 unconstrained benchmark problems, it outperformed the other 11 techniques [60]. The HH's behavior towards prey is represented by the following equations, and the concept of the HHA is properly described in [60], [61], and [62]. A flowchart for the SCL's application of the proposed HHA is given in Fig. 7.

Exploration phase:

$$Y(t+1) = \begin{cases} Y_{rabit}(t) - Y_m(t) - C_3(LB + C_4(UB - LB)), & q < .5 \\ Y_{random}(t) - C_1 \left| Y_{random}(t) - 2C_2 Y(t) \right|, & q \geq 0.5 \end{cases} \tag{24}$$

$$Y_m(t) = \frac{1}{N} \sum_{i=1}^{N} Y_i(t) \tag{25}$$

The transition from exploration to exploitation:

$$E = E_0 \left(1 - \frac{t}{T}\right) \tag{26}$$

Exploitation phase:

a) Soft besiege, $C \geq \frac{1}{2}$ *and* $|E| \geq \frac{1}{2}$

$$Y(t+1) = \Delta Y(t) - E \left| qY_{rabit}(t) - Y(t) \right| \tag{27}$$

TABLE 2. Gained PI controller gains.

Technique	Obtained PI gains	
	K_p	K_i
PI	5	100
HHA-PI (proposed)	4.0926	99.1941

where

$$\Delta Y(t) = Y_{rabit}(t) - Y(t) \tag{28}$$

b) hard besiege, $C \geq \frac{1}{2}$ *and* $|E| < \frac{1}{2}$

$$Y(t+1) = Y_{rabit}(t) - E \left| \Delta Y(t) \right| \tag{29}$$

c) soft besiege with progressive rapid dives, $C < \frac{1}{2}$ *and* $|E| \geq \frac{1}{2}$

$$H = Y_{rabit}(t) - E \left| qY_{rabit}(t) - Y(t) \right| \tag{30}$$

$$G = H + 0.01s \frac{u\sigma}{|\gamma|^{\frac{1}{\beta}}} \tag{31}$$

where

$$\sigma = \left(\frac{\Gamma(1+\beta) \sin\left(\frac{\pi\beta}{2}\right)}{\Gamma\left(\frac{1+\beta}{2}\right) \beta 2^{\left(\frac{\beta-1}{2}\right)}} \right)^{\frac{1}{\beta}} \tag{32}$$

d) hard besiege with progressive rapid dives, $C < \frac{1}{2}$ *and* $|E| < \frac{1}{2}$

$$Y(t+1) = \left\{ \begin{array}{l} H \text{ if } F(H) < F(Y(t)) \\ G \text{ if } F(G) < F(Y(t)) \end{array} \right\} \tag{33}$$

The problem formulation for the SCL is built on the objective function to minimize integral time absolute error (ITAE) given in (34) as a starting point. Table 2 shows the selected PI gains for the examined choices.

$$ITAE = \int_0^{\infty} t \left| error \right| dt \tag{34}$$

V. SIMULATED RESULTS AND DISCUSSIONS

The simulation results are run under three different WS profiles (step change, ramp, and real variations) and examined to show the efficacy of the HHA-PIC. To demonstrate the usefulness of the suggested approach, the performance of the two researched controllers is compared under all simulated situations. Additionally, the WE system efficiency is calculated over the course of the entire scenario to pinpoint the proposed controller's perfection in performing at optimal λ, C_P values under variable WSs. Table 3 lists the simulated PMSWG parameters. Moreover, the impact of the moment of inertia on the dynamic performance is given in the Appendix.

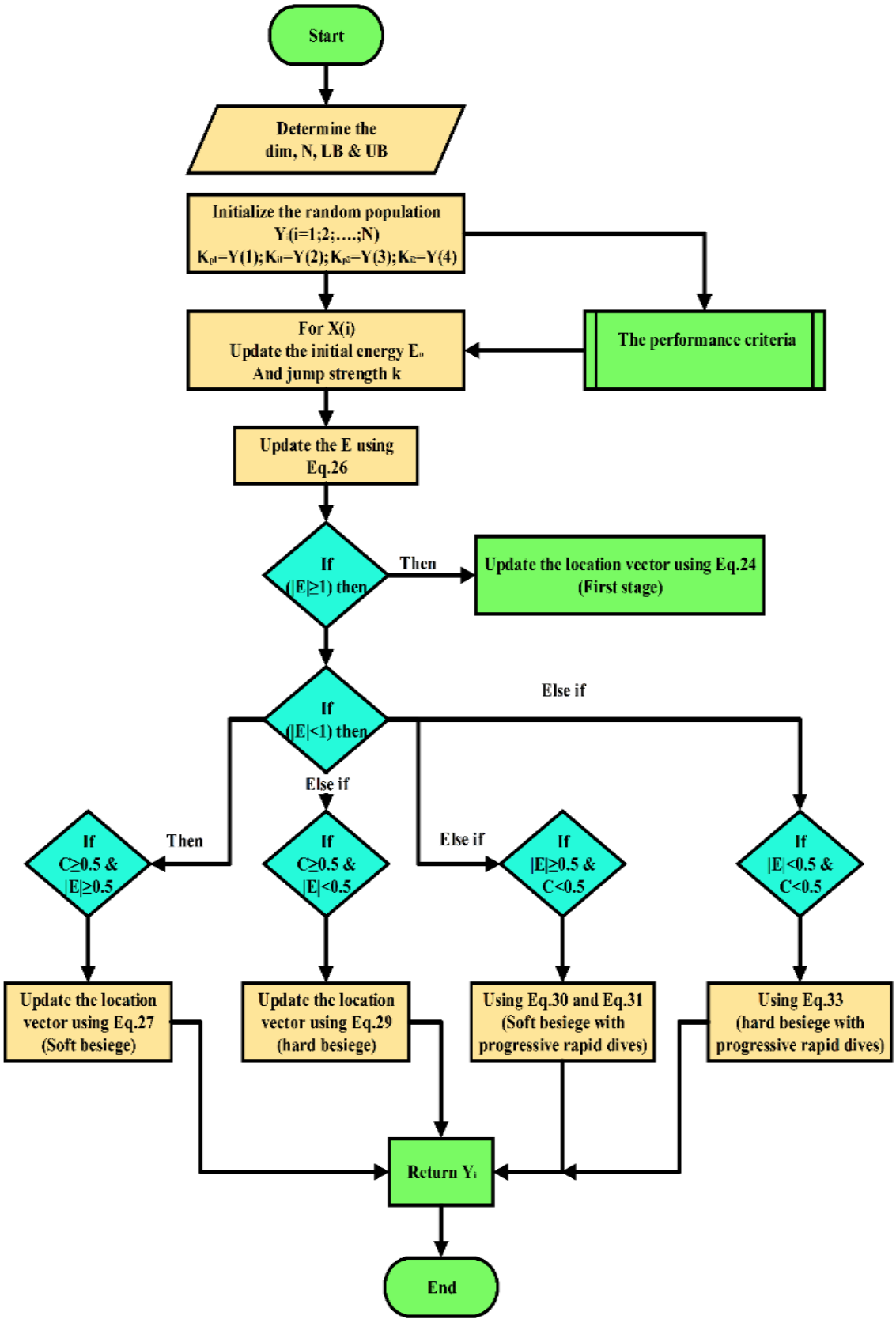

FIGURE 7. Flowchart of HHA.

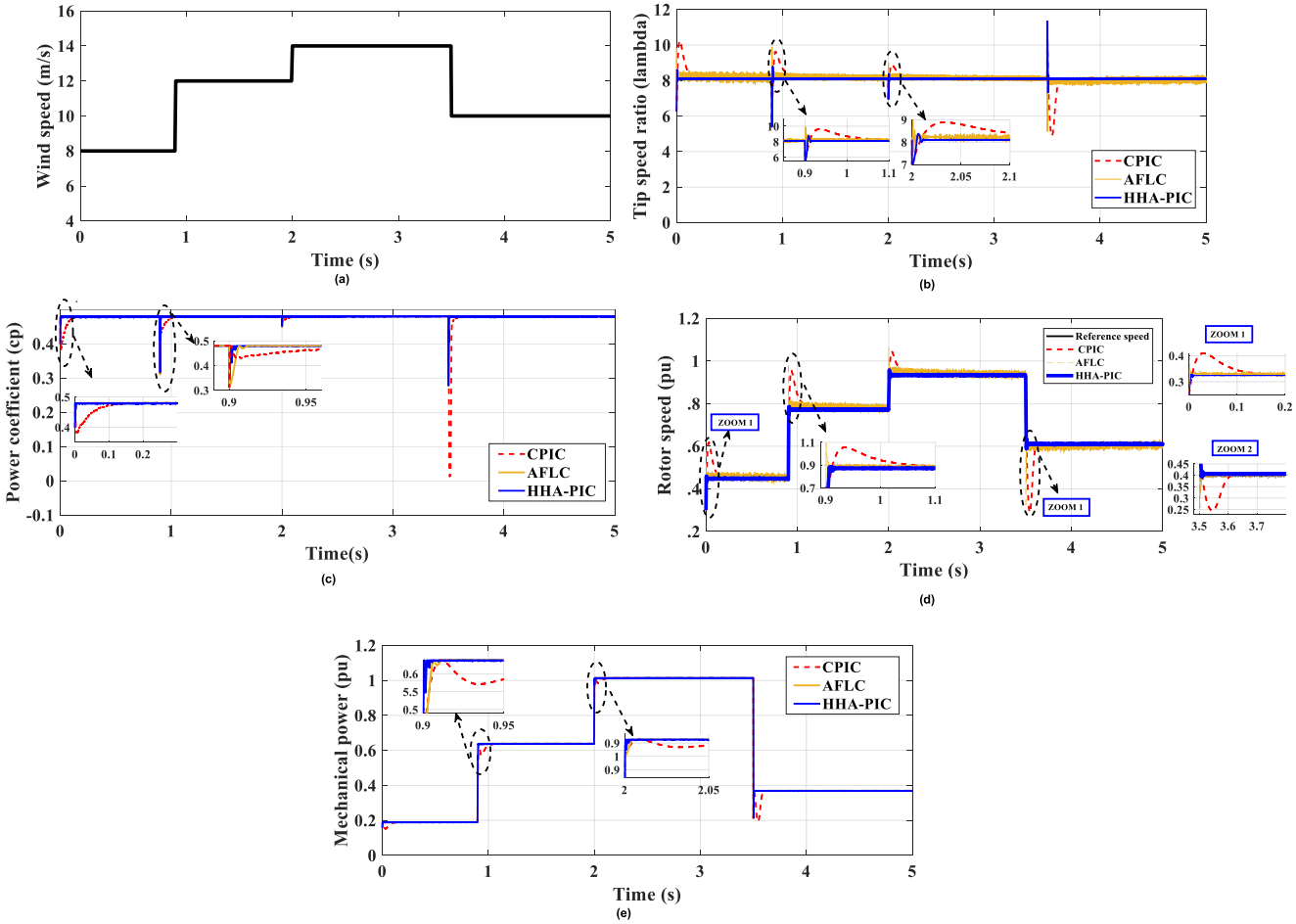

FIGURE 8. SYSTEM RESPONSE AS A RESULT OF A STEP CHANGE IN WS: (a) WS PROFILE, (b) λ, (c) C_P, (d)ω_r, (e)P_m.

TABLE 3. System parameters.

Parameters	Value and unit
Turbine blade length	2 m
Air density	1.225 kg.m^3
λ	8.1
C_P	0.48
No. of pole pairs	6
The inertia of the whole system	0.089 kg.m^2
Friction factor	0.005 N.m
DC-link voltage	750 V
The capacitance of the dc link	6000 µF
Grid frequency	60 Hz
Grid resistance	0.02 Ω
Grid inductance (L)	0.05 mH
PMSG parameters	
Nominal power (P_{nom})	10 kW
Voltage (V_{nom})	0.575 kV
Frequency (F_{nom})	60 Hz
Stator resistance (R_s)	0.00829 Ω
Stator direct inductance (L_d)	0.174 mH
Stator quadrature inductance (L_q)	0.174 mH
Permanent magnet flux (Φ)	0.071 wb

A. CASE 1: STEP CHANGE OF WS

The outcome of various turbine parameters is depicted in Fig. 8. Fig. 8 (a) depicts the studied WS profile to investigate the impacts of stepping up and down on the turbine characteristics. The settling time via CPIC, AFLC, and HHA-PIC is 0.124 s, 0.0941, and 0.0086, respectively. Fig. 8(b) and (c) show λ and $C_P$which guarantees operation at desired values (8.1 and 0.48, respectively). The CPIC reaches the optimal values λ and C_P slowly, taking 0.174 s, compared to the AFLC, taking 0.0094 s, and HHA- PIC's taking 0.0076 s. The generated P_m is displayed with all controllers and exhibits an improvement for the proposed method over the alternate in Fig. 8 (e). Figuring out how to set the ω_r to the desired value is shown in Fig. 8(d), which demonstrates how well the HHA-PIC tracks its reference than the other simulated types. Fig. 8 demonstrates how the suggested WE system can compute the P_m using the current sensor and ω_r sensor with little fluctuations. Additionally, compared to the CPIC, and AFLC, the HHA-PIC achieves maximum power with much less inaccuracy. Findings highlight the efficiency of the WSE method and the superiority of HHA-PIC over CPIC, and AFLC particularly at the beginning and changing conditions.

B. CASE 2: RAMP OF WS

In this case, the WS varies up and down with smooth ramp rates with a mean speed of 6 m/s, as seen in Fig. 9 (a), with

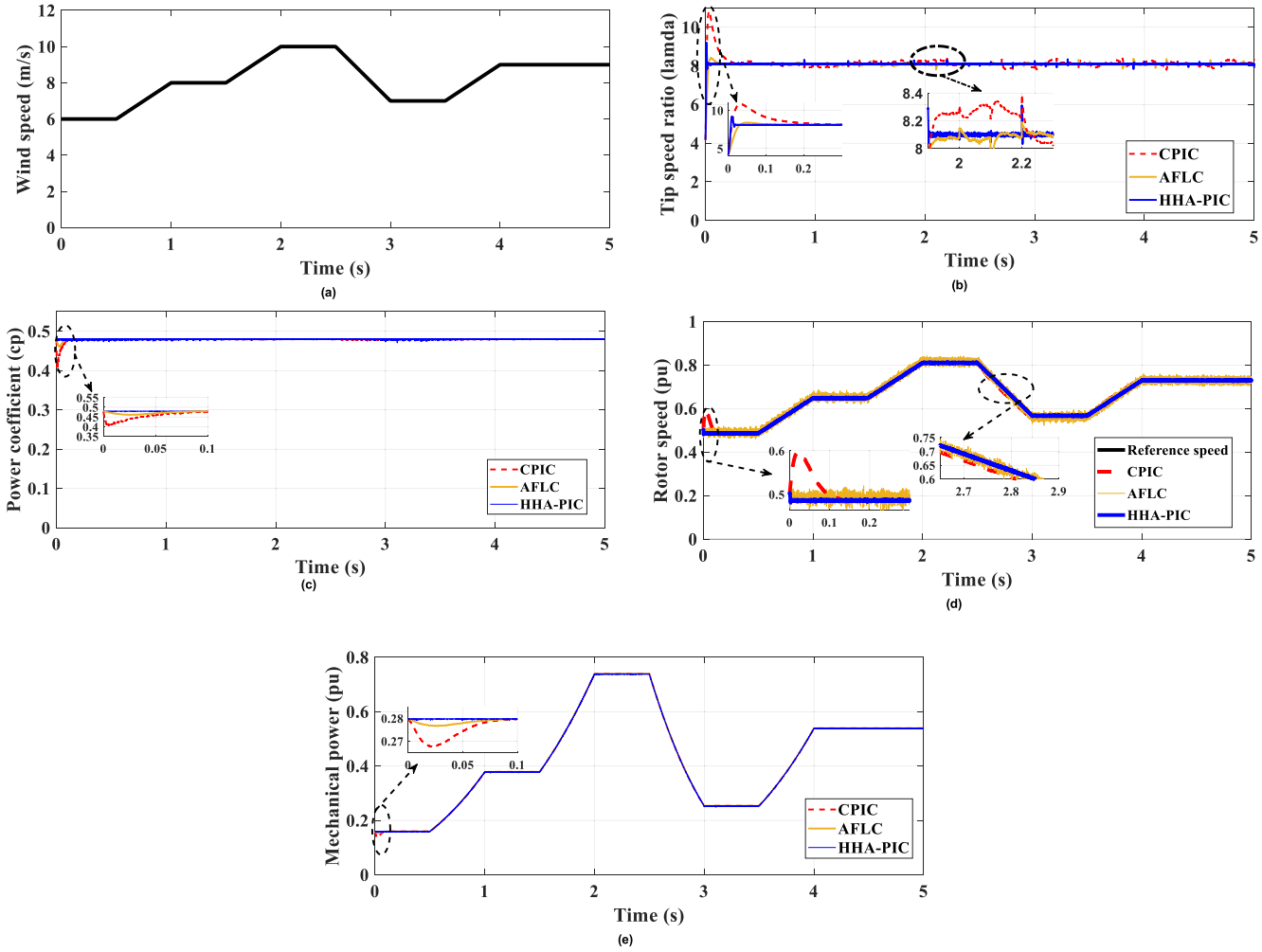

FIGURE 9. SYSTEM RESPONSE AS A RESULT OF RAMP CHANGES IN WS: (a) WS PROFILE, (b)Λ, (c) C_P, (d)ω_r, (e)P_m.

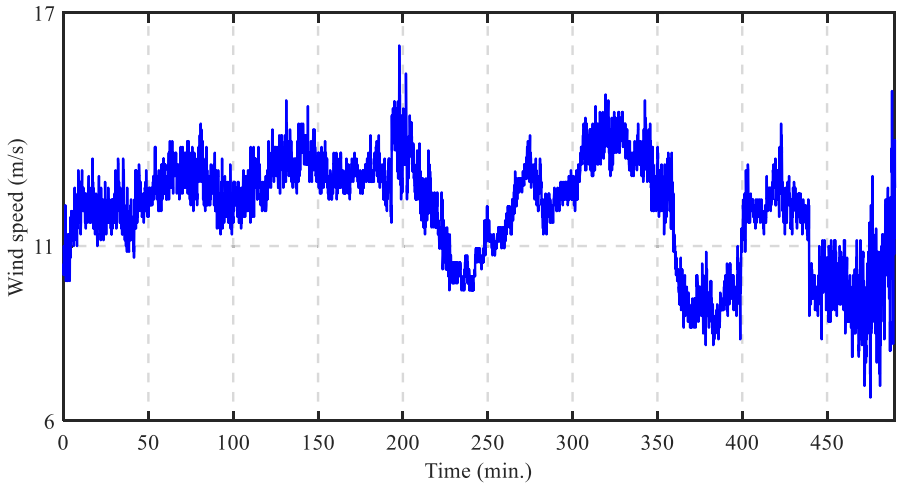

FIGURE 10. Real WS data.

a time span of 5 s. Figs.9 (b) and (c) prove that the MPPT is achieved, with the λ and C_P are maintained at their maximum and optimal values, respectively. The capability of the WSC to track the ω_r with its reference value displayed in Fig. 9(d).

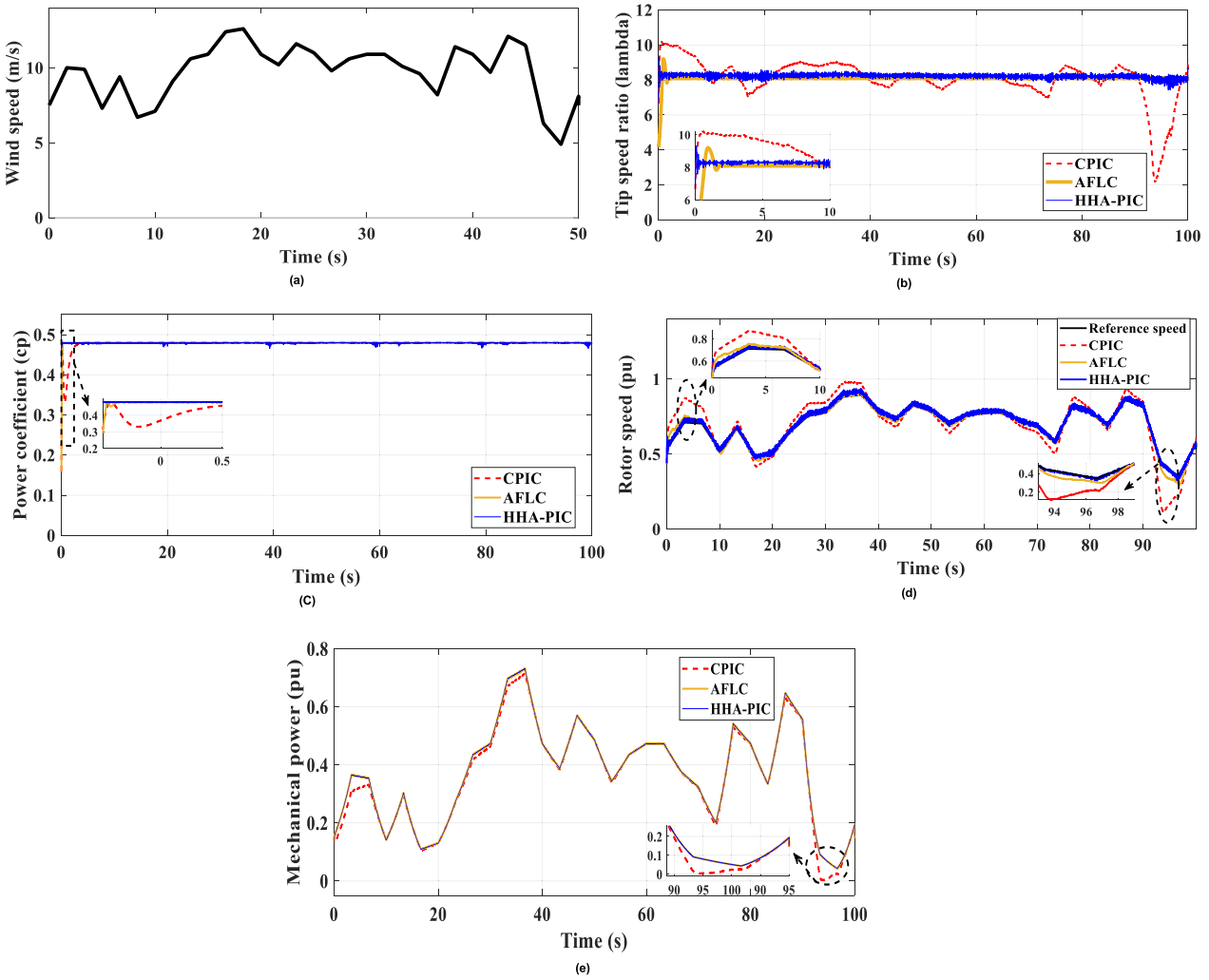

FIGURE 11. System response as a result of random variations in WS: (a) WS profile, (b)λ, (c) C_P, (d)ω_r, (e)P_m.

TABLE 4. Performance comparison with previously published techniques in PMSWG.

Refs.	Program	Machine size	Technique	Studied WS profiles	Simplicity
[64]	MATLAB	3 kW	GM-CPSO and CDW-PSO algorithms with ORB MPPT method	Step change, and random variations	×
[65]	MATLAB	250 W	Archimedes optimization algorithm	Step change, random, and real fluctuations	✓
[66]	MATLAB	1.5 MW	Super-twisting sliding mode control	Random variations only	×
[58]	MATLAB	10 kW	Adaptive FLC	Step change, and real fluctuations	×
[29]	MATLAB	10 kW	FLC	Step change, and random variations	×
[55]	MATLAB	1.5 MW	OTC, and FLC in WSC current loops.	Step change, and real fluctuations.	×
[11]	MATLAB	1.5 MW	OTC, and WOA in WSC current loops.	Step change, and random variations	✓
[56]	MATLAB	1.5 MW	WSE and MPC in SCL.	Step change only	×
Current study	MATLAB	10 kW	WSE and HHAPIC in SCL.	Step change, ramp, and real fluctuations	✓

Fig. 9(e) illustrates the captured P_m under the variations in WS. Based on the simulation results, it is clear that the system response with HHA-PIC gives better tracking capability and the oscillation rate is reduced compared to CPIC, and AFLC.

TABLE 5. IAE values for studied controllers.

ITAE	CPIC	AFLC	HHA-PIC (Proposed)
e_1 (0.9 s)	0.35	0.12	0.03
e_2 (2 s)	1.002	0.218	0.134
e_3 (3.5 s)	2.1	0.33	0.211
e_4 (5 s)	2.6	0.192	0.249
Mean Error	1.542	0.215	0.156

Fig. 9 shows that the AFLC is better than CPI in terms of less overshoot, fewer oscillations, and fast response. So, HHA-PIC can be considered very fast in response to system dynamics, particularly, when the WS changes suddenly.

C. CASE 3: REAL FLUCTUATIONS OF WS

The feasibility of the studied control system to achieve MPPT is investigated in this part. with respect to genuine WS data measured in Ras Ghareb wind farm in the Gulf of Suez, Egypt, as seen in Fig. 10. The measured data is taken for 8 hours (480 mins) and reprocessed and scaled for 100 s to fit the simulation necessities. Three controllers (CPI, AFLC, and HHA-PI) are compared to prove the efficacy of the proposed control strategy. The portrayed WS profile is displayed as given away in Fig. 11(a). Fig. 11(b) as well as Fig. 11(c) demonstrate that the MPPT is attained since the λ and C_P values are kept at their desired values, respectively. The proposed HHA-PIC for MPPT sustains the optimal C_P more rapidly and maintains the optimal value of λ as perceived in Fig. 11(b). Fig. 11(d) displays the WSC's capacity to track the ω_r with its reference value. The P_m acquired by the WS is described in Fig. 11(e). From the simulated results, it can be said that the suggested HHA-PIC makes an available option for achieving MPPT under the high variability of WS and is superior to the compared controllers.

D. SYSTEM EFFICIENCY

The efficiency of the PMSWG system using the HHA-PIC, AFLC, and CPIC is shown in Fig. 12. As can be observed from Fig. 12 (a), the HHA-PIC system outperforms the CPIC, and AFLC in terms of improving the efficiency of a WT system. According to Fig. 12 (b), the average efficiency over this time period improved to 93.91% with HHA-PIC versus 85.44% with CPIC and 93.10% with AFLC. Table 4 compares this study's findings with previously published ones to demonstrate its originality and significance.

E. ERRORS OF HHA-PIC AND CPIC BASED ON MPPT CONTROLLERS

In addition, a quantitative comparison of tracking errors using the integral of time absolute error (ITAE) for the best evaluation of the HHA-PIC method is introduced as follows [63]:

$$(\text{ITAE}) = \int_0^\infty |e(t)|\, dt \tag{35}$$

Table 5 illustrates a comparison of tracking errors of CPIC, AFLC, and HHA-PIC based on MPPT controllers. The

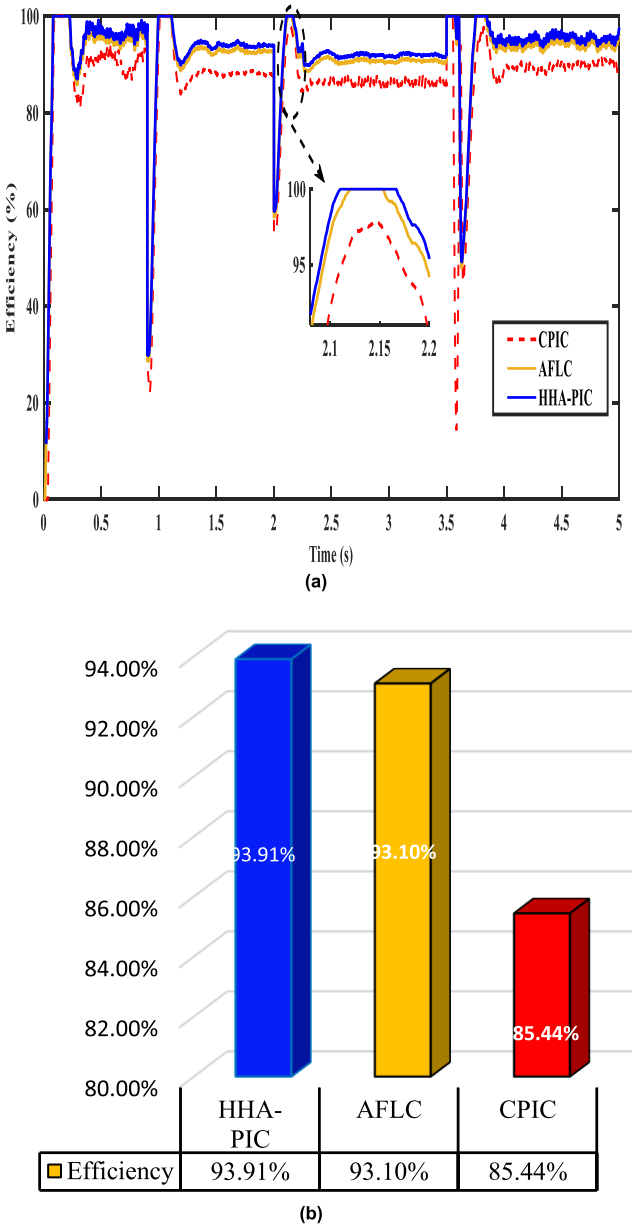

FIGURE 12. The efficiency of PMSWG under the investigated controllers.

HHA-PIC has the lowest error when compared with the other controllers. Consequently, the HHA-PIC is the best solution for achieving MPPT.

VI. CONCLUSION

This research examines a straightforward MPPT method to calculate WS without the need for any WS sensors in an effort to save installation costs and boost overall effectiveness. Additionally, the approximated WS is calculated using the ω_r and I_q feedbacks and depends on the Pm/torque. The PMSWG presents three SCL systems, the first using the CPIC, the second using AFLC, and the third using HHA-PIC. The system components and their control schemes are

also presented. The CPIC at SCL is adjusted using the AFLC and HHA approaches to fix its flaws. To control the ω_r with the required value, the HHA-PIC is implemented. The HHA-PIC, AFLC, and CPIC in SCL have been compared, and with the suggested controller, the WE system operates at Cp $=$ 0.48 and λ $=$ 8.1 in all working situations. The performance analysis demonstrates that HHA-PIC outperforms CPIC and AFLC when employing the WSE-MPPT method and suggests a significant fix for issues with traditional controllers. The overall system efficiency has been 85.44%, 93.10%, and 93.91% with the CPIC, AFLC, and HHA-PIC, respectively. Furthermore, the proposed scheme achieved higher efficiency with a negligible settling time (0.0086s). Finally, it can be said that the suggested technique improves the effectiveness and efficiency of WE systems and facilitates the production of cleaner energy.

CONFLICT OF INTEREST

The authors declare that they have no conflict of interest concerning the publication of this article.

DATA AVAILABILITY STATEMENT

Data sharing is not applicable to this article as no datasets were generated or analyzed during the current study.

APPENDIX A

Influence of inertia on electromagnetic torque [33]:

$$T_e \pm T_m = f\omega_r + J\omega_r' \tag{36}$$

(−) and (+) Signs represent acceleration and deceleration modes, respectively.

Acceleration mode ($\Delta\omega/\Delta t > 0 \Delta\omega/\Delta t > 0$)

$$T_e - T_m = f\omega_r + J\omega_r' \tag{37}$$

In step-change $\Delta t \to 0 \Delta t \to 0$ very small value, so that,

$$T_e \uparrow\uparrow \alpha J \uparrow \frac{d\omega_r}{dt} \downarrow\downarrow \alpha J \frac{\Delta\omega_r}{\Delta t} \tag{38}$$

Deceleration mode ($\Delta\omega/\Delta t < 0$)

$$T_e + T_m = f\omega_r + J\omega_r' \tag{39}$$

And,

$$T_e \downarrow\downarrow \alpha J \uparrow \frac{d\omega_r}{dt} \downarrow\downarrow \alpha J \frac{\Delta\omega_r}{\Delta t} \tag{40}$$

where $\Delta\omega = \omega_{new} - \omega_{old}$

REFERENCES

[1] *The Global Energy Market in 2020*, BP Stat. Rev. World Energy, U.K., 2021.

[2] M. Khezri, A. Heshmati, and M. Khodaei, "Environmental implications of economic complexity and its role in determining how renewable energies affect CO_2 emissions," *Appl. Energy*, vol. 306, Jan. 2022, Art. no. 117948, doi: 10.1016/j.apenergy.2021.117948.

[3] *Renewable Energy, Review World Energy Data*, BP Stat. Rev. World Energy, U.K., 2021.

[4] M. Rawa, A. Abusorrah, H. Bassi, S. Mekhilef, Z. M. Ali, S. H. E. A. Aleem, H. M. Hasanien, and A. I. Omar, "Economical-technical-environmental operation of power networks with wind-solar-hydropower generation using analytic hierarchy process and improved grey wolf algorithm," *Ain Shams Eng. J.*, vol. 12, no. 3, pp. 2717–2734, Sep. 2021, doi: 10.1016/j.asej.2021.02.004.

[5] J. K. Kaldellis and D. Apostolou, "Life cycle energy and carbon footprint of offshore wind energy. Comparison with onshore counterpart," *Renew. Energy*, vol. 108, pp. 72–84, Aug. 2017, doi: 10.1016/j.renene.2017.02.039.

[6] A. I. Omar, Z. M. Ali, M. Al-Gabalawy, S. H. E. A. Aleem, and M. Al-Dhaifallah, "Multi-objective environmental economic dispatch of an electricity system considering integrated natural gas units and variable renewable energy sources," *Mathematics*, vol. 8, no. 7, p. 1100, Jul. 2020, doi: 10.3390/math8071100.

[7] S. A. Almohaimeed, "Renewable energy opportunities and challenges in the U.S. electricity markets," *Int. Rev. Electr. Eng.*, vol. 16, no. 3, pp. 229–235, 2021, doi: 10.15866/iree.v16i3.18859.

[8] M. M. Mahmoud, M. Khalid Ratib, M. M. Aly, and A.-M.-M. Abdel-Rahim, "Wind-driven permanent magnet synchronous generators connected to a power grid: Existing perspective and future aspects," *Wind Eng.*, vol. 46, no. 1, pp. 189–199, Feb. 2022, doi: 10.1177/0309524X211022728.

[9] M. M. Hossain and M. H. Ali, "Future research directions for the wind turbine generator system," *Renew. Sustain. Energy Rev.*, vol. 49, pp. 481–489, Sep. 2015, doi: 10.1016/j.rser.2015.04.126.

[10] M. S. Meo and M. Z. A. Karim, "The role of green finance in reducing CO_2 emissions: An empirical analysis," *Borsa Istanbul Rev.*, vol. 22, no. 1, pp. 169–178, Jan. 2022, doi: 10.1016/j.bir.2021.03.002.

[11] M. M. Mahmoud, M. K. Ratib, M. M. Aly, and A.-M.-M. Abdel-Rahim, "Application of whale optimization technique for evaluating the performance of wind-driven PMSG under harsh operating events," *Process Integr. Optim. Sustain.*, vol. 6, no. 2, pp. 447–470, Jun. 2022, doi: 10.1007/s41660-022-00224-8.

[12] D. Kumar and K. Chatterjee, "A review of conventional and advanced MPPT algorithms for wind energy systems," *Renew. Sustain. Energy Rev.*, vol. 55, pp. 957–970, Mar. 2016.

[13] R. M. Linus and P. Damodharan, "Maximum power point tracking method using a modified perturb and observe algorithm for grid connected wind energy conversion systems," *IET Renew. Power Gener.*, vol. 9, no. 6, pp. 682–689, Aug. 2015, doi: 10.1049/iet-rpg.2014.0070.

[14] X. Peng, Z. Liu, and D. Jiang, "A review of multiphase energy conversion in wind power generation," *Renew. Sustain. Energy Rev.*, vol. 147, Sep. 2021, Art. no. 111172, doi: 10.1016/j.rser.2021.111172.

[15] D. Casadei, G. Serra, A. Tani, and L. Zarri, "Direct torque control for induction machines: A technology status review," in *Proc. IEEE Workshop Electr. Mach. Design, Control Diagnosis (WEMDCD)*, Mar. 2013, pp. 117–129, doi: 10.1109/WEMDCD.2013.6525172.

[16] I. Abdelsalam, G. P. Adam, D. Holliday, and B. W. Williams, "Assessment of a wind energy conversion system based on a six-phase permanent magnet synchronous generator with a twelve-pulse PWM current source converter," in *Proc. IEEE ECCE Asia Downunder*, Jun. 2013, pp. 849–854, doi: 10.1109/ECCE-Asia.2013.6579203.

[17] D. Jena and S. Rajendran, "A review of estimation of effective wind speed based control of wind turbines," *Renew. Sustain. Energy Rev.*, vol. 43, pp. 1046–1062, Mar. 2015, doi: 10.1016/j.rser.2014.11.088.

[18] S. Dolatabadi and S. Tohidi, "A review on position sensorless methods for wind generators," *Int. J. Renew. Energy Res.*, vol. 7, no. 2, pp. 476–488, 2017, doi: 10.20508/ijrer.v7i2.4923.g7083.

[19] P. Chen and D. Han, "Effective wind speed estimation study of the wind turbine based on deep learning," *Energy*, vol. 247, May 2022, Art. no. 123491, doi: 10.1016/j.energy.2022.123491.

[20] W. Qiao, W. Zhou, J. M. Aller, and R. G. Harley, "Wind speed estimation based sensorless output maximization control for a wind turbine driving a DFIG," *IEEE Trans. Power Electron.*, vol. 23, no. 3, pp. 1156–1169, May 2008, doi: 10.1109/TPEL.2008.921185.

[21] C. Emeksiz and M. Tan, "Wind speed estimation using novelty hybrid adaptive estimation model based on decomposition and deep learning methods (ICEEMDAN-CNN)," *Energy*, vol. 249, Jun. 2022, Art. no. 123785, doi: 10.1016/j.energy.2022.123785.

[22] M. A. S. Ali, K. K. Mehmood, S. Baloch, and C.-H. Kim, "Wind-speed estimation and sensorless control for SPMSG-based WECS using LMI-based SMC," *IEEE Access*, vol. 8, pp. 26524–26535, 2020, doi: 10.1109/ACCESS.2020.2971721.
[23] D. Cazau, J. Bonnel, and M. Baumgartner, "Wind speed estimation using acoustic underwater glider in a near-shore marine environment," *IEEE Trans. Geosci. Remote Sens.*, vol. 57, no. 4, pp. 2097–2106, Apr. 2019, doi: 10.1109/TGRS.2018.2871422.
[24] R. Saravanakumar and D. Jena, "Validation of an integral sliding mode control for optimal control of a three blade variable speed variable pitch wind turbine," *Int. J. Electr. Power Energy Syst.*, vol. 69, pp. 421–429, Jul. 2015, doi: 10.1016/j.ijepes.2015.01.031.
[25] A. V. P. Kumar, A. M. Parimi, and K. U. Rao, "Implementation of MPPT control using fuzzy logic in solar-wind hybrid power system," in *Proc. IEEE Int. Conf. Signal Process., Informat., Commun. Energy Syst. (SPICES)*, Feb. 2015, pp. 1–5, doi: 10.1109/SPICES.2015.7091364.
[26] X. Luo and S. Niu, "A novel contra-rotating power split transmission system for wind power generation and its dual MPPT control strategy," *IEEE Trans. Power Electron.*, vol. 32, no. 9, pp. 6924–6935, Sep. 2017, doi: 10.1109/TPEL.2016.2629021.
[27] A. Wu, B. Zhao, J. Mao, B. Wu, and F. Yu, "Adaptive active fault-tolerant MPPT control for wind power generation system under partial loss of actuator effectiveness," *Int. J. Electr. Power Energy Syst.*, vol. 105, pp. 660–670, Feb. 2019, doi: 10.1016/j.ijepes.2018.09.015.
[28] S. Ghoudelbourk, D. Dib, A. Omeiri, and A. T. Azar, "MPPT control in wind energy conversion systems and the application of fractional control (PI^{α}) in pitch wind turbine," *Int. J. Model., Identificat. Control*, vol. 26, no. 2, pp. 140–151, 2016, doi: 10.1504/IJMIC.2016.078329.
[29] A. A. Salem, N. A. N. Aldin, A. M. Azmy, and W. S. E. Abdellatif, "A fuzzy logic-based MPPT technique for PMSG wind generation system," *Int. J. Renew. Energy Res.*, vol. 9, no. 4, pp. 1751–1760, 2019, doi: 10.20508/ijrer.v9i4.10138.g7778.
[30] R. Sitharthan, T. Parthasarathy, S. S. Rani, and K. Ramya, "An improved radial basis function neural network control strategy-based maximum power point tracking controller for wind power generation system," *Trans. Inst. Meas. Control*, vol. 41, no. 11, pp. 3158–3170, Jul. 2019, doi: 10.1177/0142331218823858.
[31] X. Zhi, D. Xiangjun, and L. Lei, "MPPT for wind power system with switched reluctance generator," in *Proc. 13th IEEE Conf. Ind. Electron. Appl. (ICIEA)*, May 2018, pp. 1420–1424, doi: 10.1109/ICIEA.2018.8397932.
[32] A.-R. Youssef, H. H. H. Mousa, and E. E. M. Mohamed, "Development of self-adaptive P&O MPPT algorithm for wind generation systems with concentrated search area," *Renew. Energy*, vol. 154, pp. 875–893, Jul. 2020, doi: 10.1016/j.renene.2020.03.050.
[33] H. H. H. Mousa, A.-R. Youssef, and E. E. M. Mohamed, "Hybrid and adaptive sectors P&O MPPT algorithm based wind generation system," *Renew. Energy*, vol. 145, pp. 1412–1429, Jan. 2020, doi: 10.1016/j.renene.2019.06.078.
[34] L. Hu, F. Xue, Z. Qin, J. Shi, W. Qiao, W. Yang, and T. Yang, "Sliding mode extremum seeking control based on improved invasive weed optimization for MPPT in wind energy conversion system," *Appl. Energy*, vol. 248, pp. 567–575, Aug. 2019, doi: 10.1016/j.apenergy.2019.04.073.
[35] M. Nasiri, J. Milimonfared, and S. H. Fathi, "Modeling, analysis and comparison of TSR and OTC methods for MPPT and power smoothing in permanent magnet synchronous generator-based wind turbines," *Energy Convers. Manage.*, vol. 86, pp. 892–900, Oct. 2014, doi: 10.1016/j.enconman.2014.06.055.
[36] L. Li, B. Han, Y. Ren, J. Brindley, and L. Jiang, "An improved hybrid Hill climb searching control for MPPT of wind power generation systems under fast varying wind speed," in *Proc. IET Conf. Publications*, 2015, Art. no. CP679, doi: 10.1049/cp.2015.0493.
[37] C. Wei, Z. Zhang, W. Qiao, and L. Qu, "An adaptive network-based reinforcement learning method for MPPT control of PMSG wind energy conversion systems," *IEEE Trans. Power Electron.*, vol. 31, no. 11, pp. 7837–7848, Nov. 2016, doi: 10.1109/TPEL.2016.2514370.
[38] V. Nayanar, N. Kumaresan, and N. A. Gounden, "A single-sensor-based MPPT controller for wind-driven induction generators supplying DC microgrid," *IEEE Trans. Power Electron.*, vol. 31, no. 2, pp. 1161–1172, Feb. 2016, doi: 10.1109/TPEL.2015.2420568.
[39] A. Fathy and O. El-Baksawi, "Grasshopper optimization algorithm for extracting maximum power from wind turbine installed in Al-Jouf region," *J. Renew. Sustain. Energy*, vol. 11, no. 3, May 2019, Art. no. 033303, doi: 10.1063/1.5085167.
[40] V.-Q.-B. Ngo, M.-K. Nguyen, T.-T. Tran, Y.-C. Lim, and J.-H. Choi, "A simplified model predictive control for T-Type inverter with output LC filter," *Energies*, vol. 12, no. 1, p. 31, Dec. 2018, doi: 10.3390/en12010031.
[41] Z. Wang, J. Huang, C. Chen, and S. Fukushima, "Design of prediction-based controller for networked control systems with packet dropouts and time-delay," *Math. Problems Eng.*, vol. 2022, pp. 1–12, Jan. 2022, doi: 10.1155/2022/9437955.
[42] I. Sayedi, M. H. Fatehi, and M. Simab, "Optimal load distribution in DG sources using model predictive control and the state feedback controller for switching control," *Int. Trans. Electr. Energy Syst.*, vol. 2022, pp. 1–16, Mar. 2022, doi: 10.1155/2022/5423532.
[43] M. K. Ratib, S. Alkhalaf, T. Senjyu, A. Rashwan, M. M. Mahmoud, A. M. Hemeida, and D. Osheba, "Applications of hybrid model predictive control with computational burden reduction for electric drives fed by 3-phase inverter," *Ain Shams Eng. J.*, Oct. 2022, Art. no. 102028, doi: 10.1016/j.asej.2022.102028.
[44] M. K. Ratib and A. Rashwan, "Amplitude sampled reference-based space vector pulse width modulation for control of voltage source converters," *Energy Syst. Res.*, vol. 4, no. 2, pp. 46–63, Jul. 2021.
[45] G. Yaman and H. Y. Kanaan, "MPPT-based predictive control of a back-to-back converter for a wind power generation system," in *Proc. IEEE 12th Int. Conf. Compat., Power Electron. Power Eng. (CPE-POWERENG)*, Apr. 2018, pp. 1–7, doi: 10.1109/CPE.2018.8372512.
[46] Y. Mokhtari and D. Rekioua, "High performance of maximum power point tracking using ant colony algorithm in wind turbine," *Renew. Energy*, vol. 126, pp. 1055–1063, Oct. 2018, doi: 10.1016/j.renene.2018.03.049.
[47] A. A. Hassan and A. M. Kassem, "Speed control design of a PMSM based on functional model predictive approach," *JES. J. Eng. Sci.*, vol. 40, no. 4, pp. 1121–1135, Jul. 2012, doi: 10.21608/jesaun.2012.114483.
[48] M. Soliman, O. P. Malik, and D. T. Westwick, "Multiple model MIMO predictive control for variable speed variable pitch wind turbines," in *Proc. Amer. Control Conf.*, Jun. 2010, pp. 2778–2784, doi: 10.1109/acc.2010.5531355.
[49] M. M. Mahmoud, M. M. Aly, and A.-M.-M. Abdel-Rahim, "Enhancing the dynamic performance of a wind-driven PMSG implementing different optimization techniques," *Social Netw. Appl. Sci.*, vol. 2, no. 4, pp. 1–19, Apr. 2020.
[50] M. M. Mahmoud, "Improved current control loops in wind side converter with the support of wild horse optimizer for enhancing the dynamic performance of PMSG-based wind generation system," *Int. J. Model. Simul.*, pp. 1–15, Oct. 2022, doi: 10.1080/02286203.2022.2139128.
[51] A. I. Omar, Z. M. Ali, S. H. E. A. Aleem, E. E. A. El-Zahab, and A. M. Sharaf, "A dynamic switched compensation scheme for grid-connected wind energy systems using cuckoo search algorithm," *Int. J. Energy Convers.*, vol. 7, no. 2, pp. 64–74, 2019, doi: 10.15866/irecon.v7i2.16895.
[52] B. Ozdincer and M. Aydin, "Design of innovative radial flux permanent magnet motor alternatives with non-oriented and grain-oriented electrical steel for servo applications," *IEEE Trans. Magn.*, vol. 58, no. 2, pp. 1–4, Feb. 2022, doi: 10.1109/TMAG.2021.3078090.
[53] M. Al-Gabalawy, A. H. Elmetwaly, R. A. Younis, and A. I. Omar, "Temperature prediction for electric vehicles of permanent magnet synchronous motor using robust machine learning tools," *J. Ambient Intell. Hum. Comput.*, pp. 1–18, May 2022, doi: 10.1007/s12652-022-03888-9.
[54] A. Tounsi and H. Abid, "Generator and grid side converter control for wind energy conversion system," *Int. J. Power Electron. Drive Syst.*, vol. 12, no. 3, pp. 1832–1844, 2021, doi: 10.11591/ijpeds.v12.i3.pp1832-1844.
[55] M. M. Mahmoud, M. M. Aly, H. S. Salama, and A.-M.-M. Abdel-Rahim, "A combination of an OTC based MPPT and fuzzy logic current control for a wind-driven PMSG under variability of wind speed," *Energy Syst.*, vol. 13, no. 4, pp. 1075–1098, Nov. 2022, doi: 10.1007/s12667-021-00468-2.
[56] H. H. H. Mousa, A. Youssef, and E. E. M. Mohamed, "Model predictive speed control of five-phase permanent magnet synchronous generator-based wind generation system via wind-speed estimation," *Int. Trans. Electr. Energy Syst.*, vol. 29, no. 5, May 2019, Art. no. e2826, doi: 10.1002/2050-7038.2826.
[57] P. Kumar, S. N. Singh, and S. Dawra, "Software component reusability prediction using extra tree classifier and enhanced Harris hawks optimization algorithm," *Int. J. Syst. Assurance Eng. Manage.*, vol. 13, no. 2, pp. 892–903, Apr. 2022, doi: 10.1007/s13198-021-01359-6.

[58] M. Awad, A. M. Ibrahim, Z. M. Alaas, A. El-Shahat, and A. I. Omar, "Design and analysis of an efficient photovoltaic energy-powered electric vehicle charging station using perturb and observe MPPT algorithm," *Frontiers Energy Res.*, vol. 10, Aug. 2022, Art. no. 969482, doi: 10.3389/fenrg.2022.969482.

[59] A. A. Salem, N. A. N. Aldin, A. M. Azmy, and W. S. E. Abdellatif, "Implementation and validation of an adaptive fuzzy logic controller for MPPT of PMSG-based wind turbines," *IEEE Access*, vol. 9, pp. 165690–165707, 2021, doi: 10.1109/ACCESS.2021.3134947.

[60] Z. Yu, X. Shi, J. Zhou, X. Chen, and X. Qiu, "Effective assessment of blast-induced ground vibration using an optimized random forest model based on a Harris hawks optimization algorithm," *Appl. Sci.*, vol. 10, no. 4, p. 1403, Feb. 2020, doi: 10.3390/app10041403.

[61] A. A. Heidari, S. Mirjalili, H. Faris, I. Aljarah, M. Mafarja, and H. Chen, "Harris hawks optimization: Algorithm and applications," *Future Gener. Comput. Syst.*, vol. 97, pp. 849–872, Aug. 2019, doi: 10.1016/j.future.2019.02.028.

[62] M. M. Mahmoud, Y. M. Esmail, B. S. Atia, O. M. Kamel, K. M. AboRas, M. Bajaj, S. S. H. Bukhari, and D. E. M. Wapet, "Voltage quality enhancement of low-voltage smart distribution system using robust and optimized DVR controllers: Application of the Harris hawks algorithm," *Int. Trans. Electr. Energy Syst.*, vol. 2022, p. 18, Nov. 2022.

[63] A. E. A. Awouda and R. Bin Mamat, "Refine PID tuning rule using ITAE criteria," in *Proc. 2nd Int. Conf. Comput. Autom. Eng. (ICCAE)*, Feb. 2010, pp. 171–176, doi: 10.1109/ICCAE.2010.5451484.

[64] E. H. Dursun, H. Koyuncu, and A. A. Kulaksiz, "A novel unified maximum power extraction framework for PMSG based WECS using chaotic particle swarm optimization derivatives," *Eng. Sci. Technol., Int. J.*, vol. 24, no. 1, pp. 158–170, Feb. 2021, doi: 10.1016/j.jestch.2020.05.005.

[65] A. Fathy, A. G. Alharbi, S. Alshammari, and H. M. Hasanien, "Archimedes optimization algorithm based maximum power point tracker for wind energy generation system," *Ain Shams Eng. J.*, vol. 13, no. 2, Mar. 2022, Art. no. 101548, doi: 10.1016/j.asej.2021.06.032.

[66] M. Nasiri, S. Mobayen, and Q. M. Zhu, "Super-twisting sliding mode control for gearless PMSG-based wind turbine," *Complexity*, vol. 2019, pp. 1–15, Apr. 2019, doi: 10.1155/2019/6141607.

NOURA A. NOUR ALDIN was born in Ismailia, Egypt. She received the B.Sc. degree in industrial education from Suez University, Suez, Egypt, in 2016. She is currently an Assistant Lecturer with the Electricity Department (Electrical Power & Machines), Faculty of Technology and Education, Suez University. Her research interests include renewable energy sources, especially PV energy issues, power electronics, microgrids, and power quality.

WALID S. E. ABDELLATIF was born in Kafr El-Sheikh, Egypt. He received the B.Sc. degree in industrial education and the master's degree in industrial education in electrical power and machines from Suez Canal University, Suez, Egypt, in 2006 and 2012, respectively, and the Ph.D. degree from the Electrical Department, Faculty of Industrial Education, Suez University, Suez, in 2016. He has been an Assistant Professor with the Electricity Department (Electrical Power & Machines), Faculty of Technology and Education, Suez University, since 2016. His research interests include renewable energy sources especially wind energy issues, power electronics, microgrids, and power quality.

Z. M. SALEM ELBARBARY was born in Kafr El-Sheikh, Egypt, in April 1971. He received the B.Sc., M.Sc., and Ph.D. degrees in electrical engineering from Menoufia University, Shebin El-Kom, Egypt, in 1994, 2002, and 2007, respectively. In 2009, he joined Kafr El-Sheikh University, as an Assistant Professor. He was a Research Visitor at Ghent University, Ghent, Belgium, for two months, in 2016. He was promoted to a Full Professor in power electronics, in June 2022. His research interests include control of electrical machines, senseless control, applications of power electronics, real-time control using digital signals processing, and renewable energy applications.

AHMED I. OMAR was born in Cairo, Egypt, in September 1989. He received the B.Sc. degree (Hons.) in electrical power and machines engineering from The Higher Institute of Engineering at El-Shorouk City, Egypt, in 2011, and the M.Sc. and Ph.D. degrees in electrical power and machines from the Faculty of Engineering, Cairo University, Egypt, in 2014 and 2019, respectively. He is currently working as an Assistant Professor with The Higher Institute of Engineering at El-Shorouk City, El-Shorouk Academy. He is the author or coauthor of many refereed journals and conference papers. His research interests include renewable energy, FACTS in power systems, power quality, smart grid, energy efficiency, optimization and machine learning, green energy, and economics. He is a Reviewer for several journals, such as *Ain Shams Engineering Journal* and *Journal of Cleaner Production*.

MOHAMED METWALLY MAHMOUD was born in Sohag, Egypt. He received the B.Sc., M.Sc., and Ph.D. degrees in electrical engineering from Aswan University, Egypt, in 2015, 2019, and 2022, respectively. He is currently an Assistant Professor with Aswan University. He is the author or coauthor of many refereed journals and conference papers. He reviews for all well-known publishers (IEEE, Springer, Wiley, Elsevier, Taylor & Francis, Sage, and Hindawi). His research interests include performance improvement of wind generators, optimization methods, intelligent controllers, fault ride-through capability, power quality, FACTS tools, and energy storage systems. He has been awarded Aswan University prizes for international publishing, in 2020, 2021, and 2022, respectively.